Geophysical Research Letters

RESEARCH LETTER
10.1029/2024GL114266

Effect of Satellite Spatial Resolution on Submesoscale Variance in Ocean Color and Temperature

Luke Carberry[1], David A. Siegel[2,3], and Nicholas J. Nidzieko[2,3,4]

[1]Interdepartmental Graduate Program in Marine Science, University of California, Santa Barbara, CA, USA, [2]Earth Research Institute, University of California, Santa Barbara, CA, USA, [3]Department of Geography, University of California, Santa Barbara, CA, USA, [4]Marine Science Institute, University of California, Santa Barbara, CA, USA

Key Points:

- 1.5 km resolution satellite imagery exaggerates submesoscale variance in ocean color and temperature due to pixel noise
- High-resolution satellite imagery is a better match to theory for studying physical-biological interactions on the submesoscale

Supporting Information:

Supporting Information may be found in the online version of this article.

Correspondence to:

L. Carberry,
lcarberry@ucsb.edu

Citation:

Carberry, L., Siegel, D. A., & Nidzieko, N. J. (2025). Effect of satellite spatial resolution on submesoscale variance in ocean color and temperature. *Geophysical Research Letters*, *52*, e2024GL114266. https://doi.org/10.1029/2024GL114266

Received 18 DEC 2024
Accepted 30 DEC 2024

Author Contributions:

Conceptualization: Luke Carberry, David A. Siegel, Nicholas J. Nidzieko
Data curation: Luke Carberry
Formal analysis: Luke Carberry, Nicholas J. Nidzieko
Funding acquisition: Luke Carberry, David A. Siegel, Nicholas J. Nidzieko
Investigation: Luke Carberry, Nicholas J. Nidzieko
Methodology: Luke Carberry, David A. Siegel, Nicholas J. Nidzieko
Resources: Luke Carberry, David A. Siegel
Software: Luke Carberry
Supervision: David A. Siegel, Nicholas J. Nidzieko
Validation: Luke Carberry
Visualization: Luke Carberry
Writing – original draft: Luke Carberry

Abstract The capability of moderate-spatial-resolution satellites to accurately resolve submesoscale variations in surface tracers remains an open question, one with relevance to observing physical-biological interactions in the surface ocean. In this study, we address this question by comparing the variance of two tracers, chlorophyll concentration (Chl) and sea surface temperature (SST), resolved by two satellites—MODIS Aqua, with a resolution of 1.5 km, and Landsat 8/9, with a resolution of 30 m. We quantify tracer variance resolved by both satellites on the submesoscale using spatial variance spectral slopes. We find that MODIS measures significantly higher variance compared to Landsat, in both Chl and SST. This is because, despite higher signal-to-noise ratio for MODIS per pixel, Landsat signal-to-noise ratio increases considerably when aggregating pixels. Furthermore, by comparing Chl to SST variance for each satellite we find Landsat to be better match to theory for resolving submesoscale physical-biological interactions.

Plain Language Summary The ocean submesoscale, encompassing horizontal features from hundreds of meters to tens of kilometers in size, is known to contribute to the rapid vertical transport of heat and carbon dioxide in the surface ocean. The only sensors that can observe the surface of the ocean globally every day—satellites—have pixels that are the same size as the submesoscale: kilometers to tens of kilometers. Any noise or error in a satellite pixel will show up as real variations on these scales, leading to potentially erroneous conclusions about the contributions of ocean heat and carbon dioxide exchange to global climate. In this study, we test the effect of the spatial resolution of satellite imagery on our understanding of variations in the ocean on kilometers to tens of kilometer scales. We compare standard, kilometer-resolution satellite imagery to high-resolution imagery, and find that high-resolution satellite imagery, on the scales of tens of meters, is necessary to resolve variations in the ocean on scales of kilometers, due to the effect of satellite pixel noise. Our results serve as a guide for future work that involves understanding vertical transport in the ocean on kilometer scales.

1. Introduction

Photographs taken by astronauts aboard Gemini and Apollo in the mid-1960's first revealed the ubiquity of submesoscale currents in the ocean—eddies and fronts occurring on scales between hundreds of meters and tens of kilometers (Munk et al., 2000). Variations on this scale are unique as the velocity is not fully constrained by the Earth's rotation and vertical transport occurs (Taylor & Thompson, 2023). The submesoscale therefore presents a unique observational challenge: Submesoscale variations occur on small space and time scales (O(0.1–10) km and O(1–10) day), and yet their relation to vertical velocity means that resolving them may be critically important for understanding global climate (Taylor & Thompson, 2023).

The effects of submesoscale vertical motions have been revealed by high-resolution temporal and spatial measurements of submesoscale variability—from drifters, moorings, autonomous platforms, aircraft, ships, and satellites (e.g., Petrenko et al., 2017; Shcherbina et al., 2015). This work has shown that submesoscale vertical motions transport heat and tracers at a much greater magnitude than previously considered or characterized in global models (Zhu et al., 2024). Submesoscale vertical motions also have a significant effect on ocean primary productivity, as transport of nutrients and modulation of the mixed layer depth affect phytoplankton. But, given the observational challenges of conducting high-resolution measurements on large scales, the combined effects of submesoscale variance on phytoplankton net primary production are still not fully understood (Lévy et al., 2018).

Of the contemporary approaches to observing both physics and biology on the submesoscale, satellites remain the only means of imaging the entire ocean surface once (or more) per day. Many studies have used satellites with

Writing – review & editing:
Luke Carberry, David A. Siegel, Nicholas J. Nidzieko

spatial resolutions around 1 km or greater to detect submesoscale eddies in ocean color and sea surface temperature (SST; e.g., Buckingham et al., 2017; Gaube et al., 2019; Zhang et al., 2019). For example, variance in Chl and SST on scales between 1.5 and 10 km, resolved by the Moderate Resolution Imaging Spectroradiometer (MODIS) Aqua, was shown to account for an average of 38% of variability in the North Pacific Subtropical Gyre, suggesting that submesoscales may enhance global phytoplankton abundance (Liu & Levine, 2016).

Studies using kilometer-scale satellite products miss variability occurring on the smaller end of the submesoscale range. Study of sub-satellite-pixel variability has found that significant Chl and SST variability occurs on sub-1 km scales (Castro et al., 2017; Moses et al., 2016). To complicate things, pixel noise affects satellite imagery at the smallest resolution of the sensor, increasing uncertainty in the geophysical product (Estrella et al., 2021; Hu et al., 2000; Qi et al., 2017; Zhang et al., 2022). Despite the importance of satellites as tool for studying the submesoscale, the degree to which satellite spatial resolution biases understanding of submesoscale variance is still poorly quantified.

Here, we assess the effect of spatial resolution on submesoscale variance in Chl and SST by comparing matchups between 1.5 km MODIS and 30 m Landsat imagery. Cross-comparison between satellites has proved a useful method to improve the spatial or temporal resolution of a satellite record for a specific application (Estrella et al., 2021; Martin et al., 2024; Tang et al., 2019). Landsat's strength is high spatial resolution, with scenes limited to coastal regions at 8-day intervals, whereas MODIS provides daily, global coverage, but at lower spatial resolution (see Table S1 in Supporting Information S1). We use these two products to quantify the effectiveness of moderate-spatial-resolution satellite imagery at resolving the submesoscale using spatial variance spectral slope, which has historically been used for study of physical-biological interactions between Chl and SST (Abraham, 1998; Denman & Platt, 1976; Lévy & Klein, 2004; Lovejoy et al., 2001). Despite notable caveats in using spectral slopes to draw conclusions about processes (Armi & Flament, 1985; Franks, 2005), the method allows for comparison of variance on the specific scales over which Landsat and MODIS images overlap. Additionally, we assess the feasibility of physical-biological study for both Landsat and MODIS by comparing Chl and SST spectra. In the following section we elaborate on the sources of satellite pixel noise, followed by data collection and analysis methods. Our basic finding is that MODIS exaggerates tracer variance on the submesoscale and that, for submesoscale physical-biological analyses, Landsat tracer variance spectra are more consistent with existing theory; these results are presented in Section 3. The paper concludes with a brief discussion.

2. Methods

Methods are described briefly here; detailed methods are available in Supporting Information S1.

2.1. Pixel Noise in Satellite Imagery

Satellite pixel noise poses a critical obstacle to correctly determining Chl and SST variance on the submesoscale. When spatial variations in the signal leaving the ocean being measured by a satellite are small, for example, in between adjacent pixels, the relative amount of variation in between pixels due to instrument noise or atmospheric correction is high. Pixel noise thus causes variance spectra calculated from satellite imagery to flatten at high wavenumbers. If the pixel size is near the spatial scales of interest, that is, when using moderate-spatial-resolution satellites like MODIS to study submesoscale processes, the natural signal is obscured. This issue can be alleviated by spatially aggregating or binning satellite imagery to reduce the effect of pixel noise, increasing signal-to-noise ratio (SNR) by the square root of the number of pixels averaged (McClain et al., 2014). This method works for Landsat, because the Landsat pixel scale is much smaller than the submesoscale, such that Landsat pixels can be aggregated to produce MODIS-scale pixels at a much higher SNR than MODIS, even though MODIS SNR is higher than Landsat per pixel (Table S1 in Supporting Information S1).

2.2. Satellite Matchups, Data Processing, and Spectral Analysis

We selected four Landsat tiles to create matchup data between Landsat and MODIS (Figure S1; Table S2 in Supporting Information S1). Tiles were selected over a range of conditions and latitudes where the majority of the image was oceanic. All Landsat images for each tile with less than 20% cloud cover were acquired, and matchups were made from MODIS imagery collected within 2 hrs of these Landsat images. The same algorithms were used to calculate Chl and SST for both images. Zonal 1D spatial variance spectra were calculated using the multi-taper

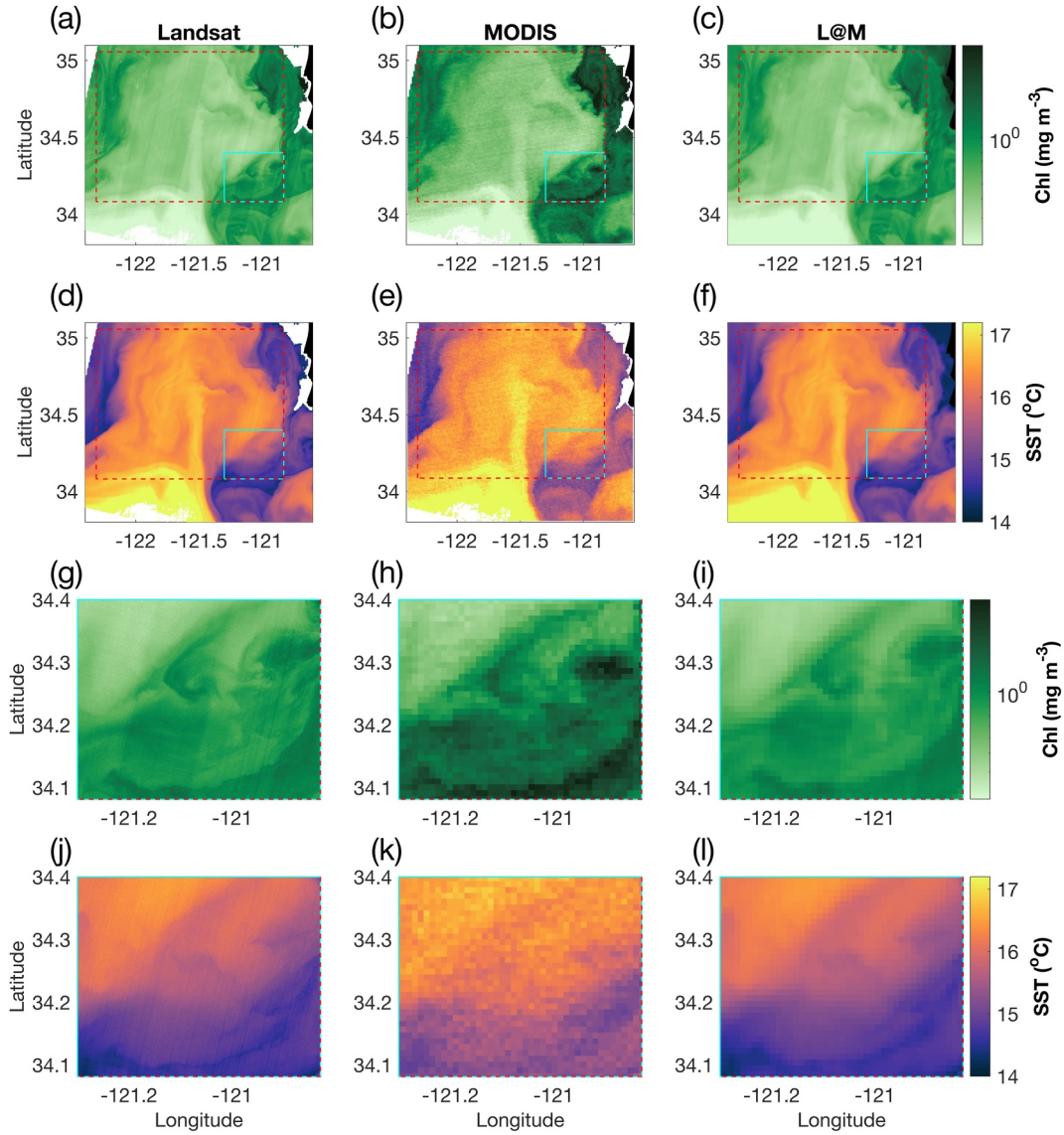

Figure 1. Chlorophyll concentration (Chl; mg m^{-3}; a–c, g–i) and sea surface temperature (SST; °C; d–f, j–l) from a Landsat 8 (left col.) and MODIS Aqua (center col.) matchup west of Point Conception, CA on 30/11/2017, with Landsat binned at MODIS resolution (L@M, right col.). Top two rows show a larger view, with coastline on the east side of the image in solid black; white areas are masked pixels. The dotted red line indicates the bounding box used for spectral analysis, and dotted cyan line indicates subregion shown in the lower two rows. For reference, the zonal length of the dotted red line is 136 km. Identical data plotted with a gray colorscale is shown in Figure S4 of Supporting Information S1.

method from linearly-detrended, horizontal transects across the largest rectangle shared between all four fields. For each image, a mean spectrum and 95% confidence intervals were calculated (Thomson & Emery, 2024). The spectral slope of each mean spectrum was calculated between the first peak in the variance-preserving spectrum (shown for Figure 2 in Figure S3 of Supporting Information S1; generally around 30 km) and 5 km; noise in the MODIS spectrum prevented using high wavenumbers.

3. Results

Qualitative comparison of a single matchup of Landsat 8 and MODIS Aqua at Point Conception, CA, reveals consistent mesoscale spatial patterns between both sensors (Figures 1a, 1b, 1d, and 1e). Examining a subregion of this image more closely, noise is visible on the scale of pixels in the MODIS imagery and is absent on those scales in the Landsat imagery (Figures 1g, 1h, 1j, and 1k). This observation is quantified by the spatial variance spectra

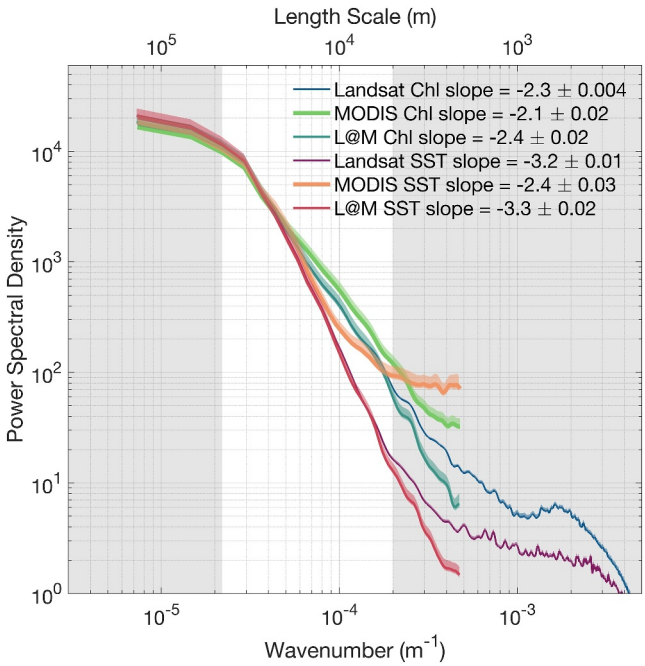

Figure 2. Average spatial variance spectra from data in Figure 1. Chl spectra are plotted in cooler tones, SST spectra are plotted in warmer tones. Thin lines are for Landsat, with increasing thickness indicating L@M and MODIS, respectively. The unshaded region between 3×10^{-5} and 2×10^{-4} m^{-1} (inverse wavenumbers of 33 and 5 km, respectively) indicates the general range over which spectral slopes were calculated (with the low wavenumber bound changing based on the variance-preserving peak). Spectra are calculated from transects with normalized units to allow comparison between °C and mg m^{-3}, giving Power Spectral Density arbitrary units of variance divided by wavenumber. 95% confidence intervals are indicated with transparent shading around each line.

of these scenes: MODIS Chl and SST slopes resemble Landsat Chl and SST slopes, respectively, on low wavenumbers, but flatten at high wavenumbers (Figure 2). In this particular example, the magnitude of the image-scale zonal gradient is greater in the MODIS image than Landsat (Figure S2 in Supporting Information S1) and so it is worth re-emphasizing that we linearly detrend the data before calculating spectra and the MODIS spectral slopes are flatter than Landsat despite this potential source of low-wavenumber variance (Figure 2).

Notably, the MODIS SST spectrum deviates from linearity in the spectral slope range (orange line in Figure 2). This is visible evidence of the combination of a red spectrum, forced by spatial variance in water-leaving radiance, with a white spectrum, caused by instrument noise. The MODIS SST spectrum follows the Landsat SST spectrum down to roughly 10 km inverse wavenumber, then begins to flatten. A linear spectral slope of −2.4 is only a rough approximation of this pattern.

When comparing all matchups across four regions (Figure 3), the difference in spatial variance between MODIS and Landsat observed in Figure 1 is generally consistent: MODIS slopes are significantly flatter than Landsat slopes for both Chl and SST (blue points in Figures 3a, and 3b; orange squares in Table 1). These results demonstrate that MODIS is measuring higher variance in Chl and SST on scales less than ∼10 km compared to Landsat.

This raises an important question: What is the source of the difference in submesoscale variance between Landsat and MODIS? Is it the effect of pixel noise? Or, is it variance at wavenumbers higher than the MODIS resolution being aliased at the pixel scale? The latter hypothesis would make it a fundamental consequence of the resolution. To answer this question, we separate the effects of spatial resolution from pixel noise by averaging Landsat observations at MODIS resolution (which we refer to hereafter as L@M). Returning to the representative example in Figure 1, L@M is visually similar to Landsat on scales of tens of kilometers. Spectral analysis reveals that L@M replicates variance in Landsat for both Chl and SST down to scales of roughly 5 km, below which L@M resolves less variance than Landsat (Figure 2). When comparing L@M to Landsat for all matchups, the L@M spectral slope was significantly steeper than Landsat on the submesoscale between 5 and 33 km (red points in Figures 3a, and 3b; orange squares in Table 1). These results indicate that a satellite sensor with 1.5 km spatial resolution, in the absence of pixel noise, resolves slightly decreased spatial variance in the ocean down to scales of 5 km, compared to a high-resolution (30 m) sensor (see Figure S5 in Supporting Information S1). In other words, the increased variance at high wavenumbers observed by MODIS is due to pixel noise, rather than aliasing of higher wavenumber variance.

Furthermore, when comparing L@M to MODIS, we found significantly different slopes between the two data sets for both Chl and SST (Figures 3c, and 3d, blue squares in Table 1). The functional difference between MODIS and L@M is the observed pixel noise in MODIS. Aggregating high-resolution imagery into a MODIS-like proxy confirms the exaggeration of submesoscale variance in Chl and SST by MODIS due to pixel noise.

From a physical-biological perspective, we next compare how each sensor resolves the relationship between Chl and SST. In the example shown in Figure 1, visually there appears to be more spatial variance within filaments and eddies in Chl than SST for both Landsat and L@M, while this pattern is slightly obscured in MODIS. This is confirmed quantitatively in the spectra. For Landsat and L@M, Chl slopes are flatter than SST slopes, indicating more variance on smaller scales for Chl than SST (Figure 2). For MODIS, the Chl spectrum is flatter than the SST spectrum from 33 km down to roughly 10 km, at which point the SST spectrum begins flattening, becoming a white spectrum on kilometer scales. The MODIS Chl spectrum also flattens at kilometer scales, but not to the same extent. Over the entire data set, Landsat and L@M showed significantly flatter Chl slopes than SST slopes (Figures 4a and 4c, green squares in Table 1), though for some images Chl slopes were steeper than SST slopes. However, we found no significant difference between MODIS Chl and SST slopes (Figure 4b, gray squares in Table 1). We surmise that

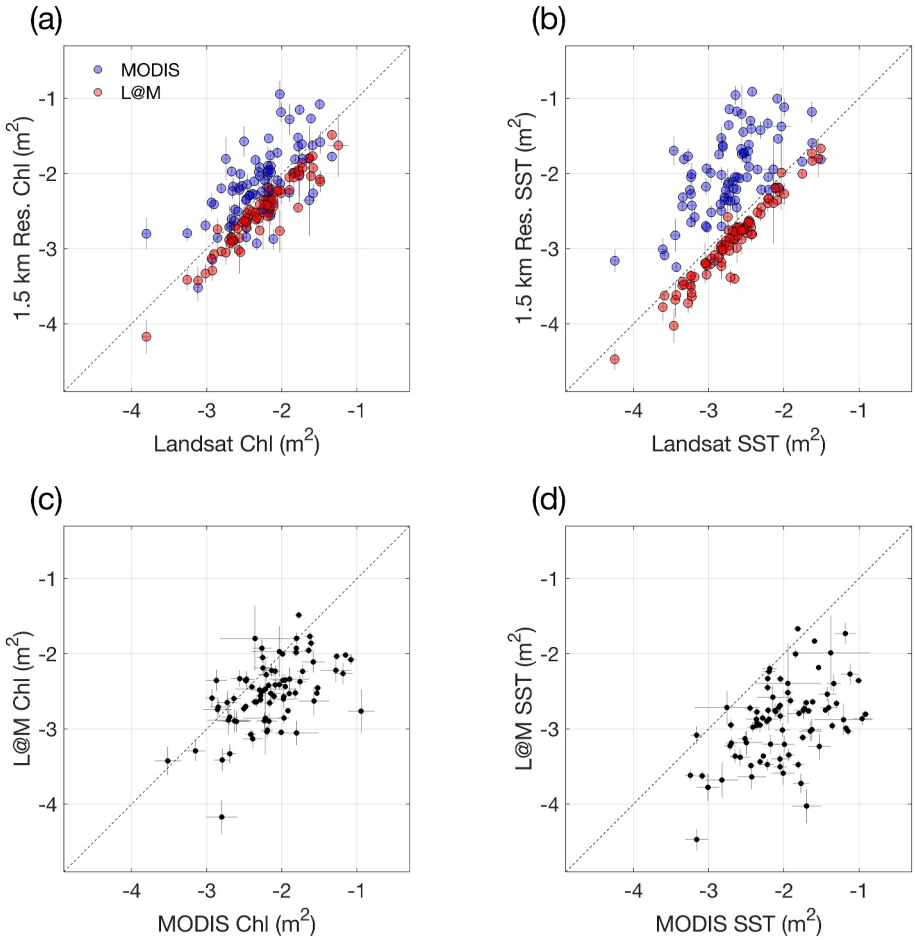

Figure 3. Intercomparison of spectral slope values from all matchups over all sites, calculated between ~33 and 5 km inverse wavenumbers. (a, b) Top row compares 30 m Landsat with 1.5 km MODIS (blue) and 1.5 km L@M (red), for Chl (left) and SST (right) data. (c, d) Bottom row shows comparison of 1.5 km data, MODIS versus L@M for Chl (left) and SST (right). Error bars indicate standard deviation.

noise in the MODIS Chl and SST spectra obscures the expected physical-biological relationship between Chl and SST (cf. Lévy & Klein, 2004).

No consistent difference in spectral slopes was found with changing latitude, likely due to size of the imagery matchup data set collected. Spectra and spectral slopes for each region specifically are shown in Figures S6–S9 of Supporting Information S1.

4. Discussion

There are two critical findings from our work: (a) The smallest scales of MODIS have more variance than Landsat at the same scales for both Chl and SST, flattening spectral slopes. Aggregating Landsat pixels to MODIS resolution suggests that this is driven by pixel noise in MODIS, not spatial resolution. (b) There is more submesoscale variance in Chl than SST, but the noise in the MODIS imagery obscures this pattern, suggesting that Landsat or other satellites that resolve the difference in spatial variance between Chl and SST should be used to study submesoscale physical-biological interactions.

We found that 1.5 km resolution, without significant instrument noise, is capable of resolving submesoscale variance in the surface ocean (between 5 and 33 km). In other words, aliasing of variance above the Nyquist wavenumber to lower wavenumbers is not a significant driver of observed variance in the satellite imagery used here. Signal-to-noise ratio, as opposed to spatial resolution, limits the utility of 1.5-km satellite data in resolving

Table 1
Spectral Slope Statistics for Matchups Between Landsat and MODIS, Including Landsat at MODIS Resolution (L@M)

	Slope Mean	Slope SD	Landsat Chl	MODIS Chl	L@M Chl	Landsat SST	MODIS SST	L@M SST
Landsat Chl	-2.25	0.16		S	F			
MODIS Chl	-2.14	0.99			F			
L@M Chl	-2.47	0.88						
Landsat SST	-2.70	0.21	F				S	F
MODIS SST	-2.01	0.79		N				F
L@M SST	-2.90	0.78			F			

Note. In columns 4–9, the spectral slopes of the row variable (left) are indicated as significantly flatter or steeper than the column variable (top) with an "F" or an "S", respectively, or an "N" if there is no significant difference (weighted paired T-test; 99% confidence; N = 76). We test two hypotheses: (1) Top right: Does pixel noise cause a difference in the same observable (Chl or SST) across platforms? Orange indicates "Yes," and blue indicates "No." (2) Bottom left: Are Chl spectral slopes significantly flatter than SST spectral slopes for a single sensor? Green indicates "Yes," and gray indicates "No.".

the submesoscale. Said a different way, SNR controls the spatial scales to which satellite data has to be aggregated in order to produce a meaningful product. Even though Landsat has lower SNR per pixel than MODIS (Table S1 in Supporting Information S1), the pixels are much smaller than the scales of interest, and thus can be aggregated to study the submesoscale at high fidelity.

In terms of understanding physical-biological interactions, our Landsat data set confirms what has been predicted by early modeling work that flatter spectral slopes should occur for Chl than SST; this may be due to either internal biological processes (Abraham, 1998; Denman et al., 1977) or purely external physical processes (Lévy & Klein, 2004). Observational work via in situ transect observations (Denman & Platt, 1976; Lovejoy et al., 2001;

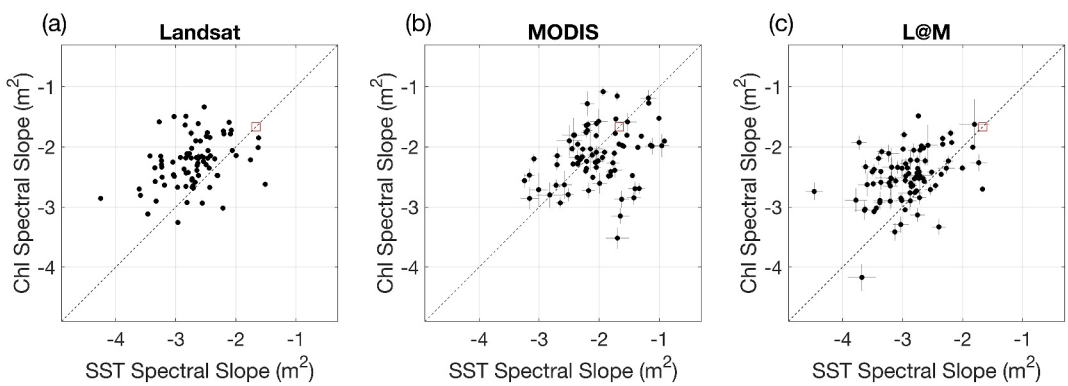

Figure 4. Comparison of Chl versus SST spectral slopes for all four regions calculated between ~33 and 5 km inverse wavenumber: (a) Landsat, (b) MODIS, and (c) Landsat at MODIS resolution. −5/3 is indicated with a red square on the 1:1 line. Spectra and spectral slopes for each region individually are shown in Figures S6–S9 of Supporting Information S1. Error bars indicate standard deviation (Landsat error bars are smaller than the marker).

A. P. Martin and Srokosz, 2002; van Gennip et al., 2016) and satellite imagery (Denman & Abbott, 1994; Smith et al., 1988) has generally borne out these predictions. However, previous satellite studies of Chl and SST on the submesoscale has been conducted with satellites that have $O(1)$ km resolution, for example, MODIS, SeaWIFS, and CZCS (Denman & Abbott, 1994; Smith et al., 1988). As noted, the submesoscale occurs at the high-wavenumber limit of those sensors, making the differences in spatial variance between Chl and SST difficult to distinguish due to pixel noise. Notably, geostatistical analysis of MODIS Chl reveals considerable unresolved variability on $O(100)$ km scales, due to either noise or submesoscale variability (Doney et al., 2003; Glover et al., 2018). Our work highlights the importance of either high SNR or high spatial resolution in resolving the submesoscale.

Passive remote sensing is inherently photon-limited, as there are tradeoffs between spatial resolution, spectral resolution, SNR, and repeat time. High-spatial-resolution satellites designed primarily for terrestrial remote sensing–like Landsat and Sentinel–exchange repeat time and SNR for high spatial resolution. Time scales of variability on land are long, and land targets are bright. With the ocean being a temporally-variable, dark target, the necessity of rapid repeat times and high SNR must come at the expense of either decreased spatial resolution or decreased spectral resolution. Constellations of satellites, like Landsat 8/9, have shown the possibility of making high-SNR, high-spatial-resolution observations at rapid repeat times, albeit at moderate spectral resolution. Similarly, technological and design advancements have enabled hyperspectral resolution for Plankton, Aerosol, Cloud, ocean Ecosystem (PACE) at a similar spatial resolution, SNR, and repeat time to MODIS (Werdell et al., 2019). With PACE's hyperspectral resolution, wavelengths can be aggregated to produce excellent SNRs at a similar spectral resolution to MODIS. Our findings emphasize that the SNR of moderate-spatial-resolution satellite sensors like PACE is critical in their ability to resolve submesoscale variations in ocean color and temperature.

Data Availability Statement

Data produced by NASA's MODIS Aqua and Landsat 8 and 9 satellites was used in the creation of this manuscript. A complete list of matchup images and locations, accompanied by imagery used in Figures 1 and 2, and calculated variance spectra used in Figures 3 and 4, and Table 1, along with all necessary code is available (Carberry, 2024).

Acknowledgments
The authors would like to thank Sasha Kramer, Patrick Gray, and Tom Bell, for helpful conversations regarding the paper, and both reviewers for helpful comments. The authors would also like to thank the team at the NASA Goddard Space Flight Center, especially the Ocean Biology Processing Group, for developing and supporting the array of earth-observing satellites that have dramatically improved the field's understanding of the ocean. Graduate funding was provided by the Department of Defense National Defense Science and Engineering Graduate Fellowship and the UC Chancellor's Fellowship. Support for this study was provided by grants from the National Science Foundation (NSF OCE-2022748) and the Office of Naval Research (ONR N00014-20-1-2566).

References

Abraham, E. R. (1998). The generation of plankton patchiness by turbulent stirring. *Nature*, *391*(6667), 577–580. https://doi.org/10.1038/35361

Armi, L., & Flament, P. (1985). Cautionary remarks on the spectral interpretation of turbulent flows. *Journal of Geophysical Research*, *90*(C6), 11779–11782. https://doi.org/10.1029/jc090ic06p11779

Buckingham, C. E., Khaleel, Z., Lazar, A., Martin, A. P., Allen, J. T., Naveira, A. C., et al. (2017). Testing Munk's hypothesis for submesoscale eddy generation using observations in the North Atlantic. *Journal of Geophysical Research: Oceans*, *122*(8), 6725–6745. https://doi.org/10.1002/2017jc012910

Carberry, L. (2024). Lukecarberry/subm_variance_spectra: Data repository for manuscript (Version 1) [Dataset]. *Zenodo*. https://doi.org/10.5281/zenodo.11586524

Castro, S., Emery, W., Wick, G., & Tandy, W. (2017). Submesoscale Sea surface temperature variability from UAV and satellite measurements. *Remote Sensing*, *9*(11), 1089. https://doi.org/10.3390/rs9111089

Denman, K., Okubo, A., & Platt, T. (1977). The chlorophyll fluctuation spectrum in the sea 1, 2. *Limnology and Oceanography*, *22*(6), 1033–1038.

Denman, K. L., & Abbott, M. R. (1994). Time scales of pattern evolution from cross-spectrum analysis of advanced very high resolution radiometer and coastal zone color scanner imagery. *Journal of Geophysical Research*, *99*(C4), 7433–7442. https://doi.org/10.1029/93jc02149

Denman, K. L., & Platt, T. (1976). The variance spectrum of phytoplankton in a turbulent ocean. *Journal of Marine Research*, *34*(4), 593–601.

Doney, S. C., Glover, D. M., McCue, S. J., & Fuentes, M. (2003). Mesoscale variability of Sea-viewing Wide Field-of-view Sensor (SeaWiFS) satellite ocean color: Global patterns and spatial scales. *Journal of Geophysical Research*, *108*(C2). https://doi.org/10.1029/2001jc000843

Estrella, E. H., Gilerson, A., Foster, R., & Groetsch, P. (2021). Spectral decomposition of remote sensing reflectance variance due to the spatial variability from ocean color and high-resolution satellite sensors. *Journal of Applied Remote Sensing*, *15*(2), 024522. https://doi.org/10.1117/1.jrs.15.024522

Franks, P. J. S. (2005). Plankton patchiness, turbulent transport and spatial spectra. *Marine Ecology Progress Series*, *294*, 295–309. https://doi.org/10.3354/meps294295

Gaube, P., Chickadel, C. C., Branch, R., & Jessup, A. (2019). Satellite observations of SST-induced wind speed perturbation at the oceanic submesoscale. *Geophysical Research Letters*, *46*(5), 2690–2695. https://doi.org/10.1029/2018gl080807

Glover, D. M., Doney, S. C., Oestreich, W. K., & Tullo, A. W. (2018). Geostatistical analysis of mesoscale spatial variability and error in SeaWiFS and MODIS/Aqua global ocean color data. *Journal of Geophysical Research: Oceans*, *123*(1), 22–39. https://doi.org/10.1002/2017jc013023

Hu, C., Carder, K. L., & Müller-Karger, F. E. (2000). How precise are SeaWiFS ocean color estimates? Implications of digitization-noise errors. *Remote Sensing of Environment*, *76*(2), 239–249. https://doi.org/10.1016/s0034-4257(00)00206-6

Lévy, M., Franks, P. J. S., & Smith, K. S. (2018). The role of submesoscale currents in structuring marine ecosystems. *Nature Communications*, *9*(1), 4758. https://doi.org/10.1038/s41467-018-07059-3

Lévy, M., & Klein, P. (2004). Does the low frequency variability of mesoscale dynamics explain a part of the phytoplankton and zooplankton spectral variability? *Proceedings of the Royal Society A: Mathematical, Physical and Engineering Sciences*, *460*(2046), 1673–1687. https://doi.org/10.1098/rspa.2003.1219

Liu, X., & Levine, N. M. (2016). Enhancement of phytoplankton chlorophyll by submesoscale frontal dynamics in the North Pacific Subtropical Gyre. *Geophysical Research Letters*, *43*(4), 1651–1659. https://doi.org/10.1002/2015gl066996

Lovejoy, S., Currie, W. J. S., Tessier, Y., Claereboudt, M. R., Bourget, E., Roff, J. C., & Schertzer, D. (2001). Universal multifractals and ocean patchiness: Phytoplankton, physical fields and coastal heterogeneity. *Journal of Plankton Research*, *23*(2), 117–141. https://doi.org/10.1093/plankt/23.2.117

Martin, A. P., & Srokosz, M. A. (2002). Plankton distribution spectra: Inter-size class variability and the relative slopes for phytoplankton and zooplankton. *Geophysical Research Letters*, *29*(24), 2213. https://doi.org/10.1029/2002gl015117

Martin, S. A., Manucharyan, G. E., & Klein, P. (2024). Deep learning improves global satellite observations of ocean eddy dynamics. *Geophysical Research Letters*, *51*(17), e2024GL110059. https://doi.org/10.1029/2024gl110059

McClain, C. R., Meister, G., & Monosmith, B. (2014). Chapter 2.1—satellite Ocean Color sensor design concepts and performance requirements. In G. Zibordi, C. J. Donlon, & A. C. Parr (Eds.), *Experimental methods in the physical sciences—47*. Academic Press. Retrieved from. https://doi.org/10.1016/B978-0-12-417011-7.00005-2

Moses, W. J., Ackleson, S. G., Hair, J. W., Hostetler, C. A., & Miller, W. D. (2016). Spatial scales of optical variability in the coastal ocean: Implications for remote sensing and in situ sampling. *Journal of Geophysical Research: Oceans*, *121*(6), 4194–4208. https://doi.org/10.1002/2016jc011767

Munk, W., Armi, L., Fischer, K. W., & Zachariasen, F. (2000). Spirals on the sea. *Proceedings of the Royal Society A: Mathematical, Physical and Engineering Sciences*, *456*(1997), 1217–1280. https://doi.org/10.1098/rspa.2000.0560

Petrenko, A. A., Doglioli, A. M., Nencioli, F., Kersalé, M., Hu, Z., & d'Ovidio, F. (2017). A review of the LATEX project: Mesoscale to submesoscale processes in a coastal environment. *Ocean Dynamics*, *67*(3–4), 513–533. https://doi.org/10.1007/s10236-017-1040-9

Qi, L., Lee, Z., Hu, C., & Wang, M. (2017). Requirement of minimal signal-to-noise ratios of ocean color sensors and uncertainties of ocean color products. *Journal of Geophysical Research: Oceans*, *122*(3), 2595–2611. https://doi.org/10.1002/2016jc012558

Shcherbina, A. Y., Sundermeyer, M. A., Kunze, E., D'Asaro, E. A., Badin, G., Birch, D. W., et al. (2015). The LatMix summer campaign: Submesoscale stirring in the upper ocean. *American Meteorological Society*, *96*(8), 1257–1279. https://doi.org/10.1175/bams-d-14-00015.1

Smith, R. C., Zhang, X., & Michaelsen, J. (1988). Variability of pigment biomass in the California current system as determined by satellite imagery: 1. Spatial variability. *Journal of Geophysical Research*, *93*(D9), 10863–10882. https://doi.org/10.1029/jd093id09p10863

Tang, R., Shen, F., Pan, Y., Ruddick, K., & Shang, P. (2019). Multi-source high-resolution satellite products in Yangtze Estuary: Cross-comparisons and impacts of signal-to-noise ratio and spatial resolution. *Optics Express*, *27*(5), 6426–6441. https://doi.org/10.1364/oe.27.006426

Taylor, J. R., & Thompson, A. F. (2023). Submesoscale dynamics in the upper ocean. *Annual Review of Fluid Mechanics*, *55*(1), 103–127. https://doi.org/10.1146/annurev-fluid-031422-095147

Thomson, R. E., & Emery, W. J. (2024). *Data analysis methods in physical oceanography*. Elsevier.

van Gennip, S., Martin, A. P., Srokosz, M. A., Allen, J. T., Pidcock, R., Painter, S. C., & Stinchcombe, M. C. (2016). Plankton patchiness investigated using simultaneous nitrate and chlorophyll observations. *Journal of Geophysical Research: Oceans*, *121*(6), 4149–4156. https://doi.org/10.1002/2016jc011789

Werdell, P. J., Behrenfeld, M. J., Bontempi, P. S., Boss, E., Cairns, B., Davis, G. T., et al. (2019). The plankton, aerosol, cloud, ocean ecosystem mission: Status, science, advances. *Bulletin of the American Meteorological Society*, *100*(9), 1775–1794. https://doi.org/10.1016/j.rse.2012.07.012

Zhang, M., Ibrahim, A., Franz, B., Ahmad, Z., & Sayer, A. (2022). Estimating pixel-level uncertainty in ocean color retrievals from MODIS. *Optics Express*, *30*(17), 31415. https://doi.org/10.1364/oe.460735

Zhang, Y., Hu, C., Liu, Y., Weisberg, R. H., & Kourafalou, V. H. (2019). Submesoscale and mesoscale eddies in the Florida straits: Observations from satellite Ocean Color measurements. *Geophysical Research Letters*, *46*(22), 13262–13270. https://doi.org/10.1029/2019gl083999

Zhu, R., Yang, H., Li, M., Chen, Z., Ma, X., Cai, J., & Wu, L. (2024). Observations reveal vertical transport induced by submesoscale front. *Scientific Reports*, *14*(1), 4407. https://doi.org/10.1038/s41598-024-54940-x

References From the Supporting Information

Chang, T. (2023). *MODIS TEB calibration and performance*. MODIS Characterization Support Team, NASA GSFC. Retrieved from https://modis.gsfc.nasa.gov/sci_team/meetings/202305/calibration.php

Cook, M., Schott, J., Mandel, J., & Raqueno, N. (2014). Development of an operational calibration methodology for the landsat thermal data archive and initial testing of the atmospheric compensation component of a Land Surface Temperature (LST) product from the archive. *Remote Sensing*, *6*(11), 11244–11266. https://doi.org/10.3390/rs61111244

ESA Copernicus. (2024). SentiWiki sentinel-3 SLSTR instrument. Retrieved from https://sentiwiki.copernicus.eu/web/s3-slstr-instrument

Haentjens, N., & Bourdin, G. (2020). getOC. Retrieved from https://github.com/OceanOptics/getOC

Irons, J. R., Dwyer, J. L., & Barsi, J. A. (2012). The next Landsat satellite: The Landsat data continuity mission. *Remote Sensing of Environment*, *122*, 11–21.

Kilpatrick, K., & Baker-Yeboah, S. (2016). Climate Data Record (CDR) program. Climate Algorithm Theoretical Basis Document (C-ATBD). *Sea Surface Temperature – Pathfinder* (*0099*). Retrieved from https://www.ncei.noaa.gov

Kilpatrick, K. A., Podestá, G., Walsh, S., Williams, E., Halliwell, V., Szczodrak, M., et al. (2015). A decade of sea surface temperature from MODIS. *Remote Sensing of Environment*, *165*, 27–41. https://doi.org/10.1016/j.rse.2015.04.023

McClain, C. R., Meister, G., & Monosmith, B. (2014). Chapter 2.1 - satellite ocean color sensor design concepts and performance requirements. In G. Zibordi, C. J. Donlon, & A. C. Parr (Eds.), *Experimental methods in the physical sciences–47*. Academic Press. https://doi.org/10.1016/B978-0-12-417011-7.00005-2

Mobley, C. D., Werdell, J., Franz, B., Ahmad, Z., & Bailey, S. (2016). Atmospheric correction for satellite ocean color radiometry. *NTRS–NASA Technical Reports Server. Goddard Space Flight Center: NASA*. Retrieved from https://ntrs.nasa.gov/citations/20160011399

Motohka, T., Nasahara, K. N., Murakami, K., & Nagai, S. (2011). Evaluation of sub-pixel cloud noises on MODIS daily spectral indices based on in situ measurements. *Remote Sensing*, *3*(8), 1644–1662. https://doi.org/10.3390/rs3081644

O'Reilly, J. E., & Werdell, P. J. (2019). Chlorophyll algorithms for ocean color sensors - OC4, OC5 & OC6. *Remote Sensing of Environment*, *229*, 32–47. https://doi.org/10.1016/j.rse.2019.04.021

Perez, C. (2021). *S-NPP/N20 VIIRS thermal emissive bands on-orbit performance and calibration*. VIIRS Characterization Support Team, NASA GSFC. Retrieved from https://modis.gsfc.nasa.gov/sci_team/meetings/202102/presentations.php

Seibold, P. (2020). Largest inscribed rectangle square or circle. *MATLAB Central File Exchange*. https://in.mathworks.com/matlabcentral/fileexchange/71491-largest-inscribed-rectangle-square-or-circle

Wiens, T. (2024). Peak interpolation. MATLAB central file exchange. https://www.mathworks.com/matlabcentral/fileexchange/24465-peak-interpolation

Wu, F., Cornillon, P., Boussidi, B., & Guan, L. (2017). Determining the pixel-to-pixel uncertainty in satellite-derived SST fields. *Remote Sensing*, *9*(9), 877. https://doi.org/10.3390/rs9090877

Zhang, M., Ibrahim, A., Franz, B., Ahmad, Z., & Sayer, A. (2022). Estimating pixel-level uncertainty in ocean color retrievals from MODIS. *Optics Express*, *30*(17), 31415. https://doi.org/10.1364/oe.460735